J Clust Sci (2016) 27:1989–1999
DOI 10.1007/s10876-016-1062-3

ORIGINAL PAPER

Synthesis and Catalytic Evaluation of Silver Nanoparticles Synthesized with *Aloysia triphylla* Leaf Extract

J. Luis López-Miranda[1] · S. E. Borjas-Garcia[2] · R. Esparza[3] · G. Rosas[1]

Received: 4 July 2016 / Published online: 19 August 2016

Abstract In this investigation, we report the biosynthesis of the silver nanoparticles using *Aloysia triphylla* leaves extract. The as-prepared silver nanoparticles were characterized by ultraviolet–visible (Uv–vis) spectroscopy, X-ray diffractometry, scanning electron microscopy and transmission electron microscopy The infrared spectroscopy (FTIR) and Raman spectroscopy techniques were also used to evaluate the chemical groups of the plant extract involved in the silver ions bioreduction. The results indicate that as the plant extract/precursor salt ratio increases, the size of the nanoparticles decreases. Also, as the reaction temperature increases, the reduction rate increased too, resulting in the formation of smaller nanoparticles-size ranges. Uv–vis spectroscopy illustrates absorption peaks in the range of wavelengths of 430–445 nm corresponding to surface plasmon resonance band of silver nanoparticles. The X-ray diffraction (XRD) confirmed the presence of silver solids with fcc structure type. The FTIR analysis showed that the bands corresponding to phenolic compounds and the amide group were involved in the synthesis and stabilization of silver nanoparticles, respectively. The Raman studies showed bands at 1380 and 1610 cm^{-1}, which correspond to the aromatic and amide compounds, confirming the FTIR results. The Uv–vis results indicate the capacity of silver nanoparticles to reduce the methylene blue.

✉ J. Luis López-Miranda
lopezfim@gmail.com

[1] Instituto de Investigaciones Metalúrgicas, UMSNH, edificio U, ciudad universitaria, C.P. 58060 Morelia, Michoacán, Mexico

[2] Instituto de Física y Matemáticas, UMSNH, ciudad universitaria, C.P. 58060 Morelia, Michoacán, Mexico

[3] Centro de Física Aplicada y Tecnología Avanzada, Universidad Nacional Autónoma de México, Boulevard Juriquilla 3001, C.P. 76230 Santiago De Querétaro, Querétaro, Mexico

Keywords Silver nanoparticles · Biosynthesis · *Aloysia triphylla* · Methylene blue reduction · Structural characterization

Introduction

In recent years, interest in metallic nanoparticles has been growing steadily due to their unique properties and applications [1–3]. Specifically, silver nanoparticles (AgNPs) have been used in various fields as, for example, antibacterial [4–7], catalytic [8–11], larvicidal, or mosquitocidal [12–15] agents. There are several ways of synthesizing the nanoparticles, such as physical, chemical, or biological methods. However, the chemical methods are expensive and involve toxic reagents [16–18]. Sodium borohydride and sodium citrate are some of the hazardous reactants employed in this kind of synthesis [19]. Moreover, several solvents are used, for example, dimethylformamide, ethylene glycol, toluene, and chloroform [20]. These substances contaminate the nanoparticles, reducing their potential applications, especially in the field of medicine. On the other hand, the synthesis of nanoparticles by physical methods is expensive, and they are carried out with a great consumption of energy, at high temperatures, and under high pressures [21]. Some examples of these methods are milling, sputtering, and laser ablation [19]. Finally, the biological or green synthesis methods are emerging and promising techniques. This kind of synthesis consists in preparing metal nanoparticles using plants [22], seeds [23], bacteria [24], fungi [25], and algae [26]. The role of the organism is to provide stabilizing agents and reducing agents for nanoparticle synthesis. However, some of these methods have disadvantages. For example, the synthesis of nanoparticles using microbial is expensive and, in some cases, produces dangerous products [27]. Among all the green synthesis, the use of plants is the most commonly employed method for nanoparticle preparation. Some advantages to this approach are the low cost, simplicity, non-toxicity, easy availability, and potential for large-scale production [27, 28]. Moreover, the plant extracts have a higher bioreduction potential than the bacteria [27]. Several plants have been used in the synthesis of silver nanoparticles using leaf extracts [29–31]. To our knowledge, the *Aloysia triphylla* (*A. triphylla*) plant extract has not been employed in the past for the nanoparticle synthesis. The extract of *A. triphylla* leaves has spasmolytic, sedative, stomachic, diuretic, and antispasmodic properties [32] due to its high levels of flavonoids, terpenoids, and phenolic compounds, which have reducing capabilities [33]. According to Olmedo et al., the main components of *A. triphylla* leaves are spathulenol, geranial, and neral. The first is a sesquiterpene, and the other compounds are terpenoids [34]. All these compounds have reducing activity using hydrogen or electron transfer [35].

On the other hand, the methylene blue is an organic dye employed in the textile and paper industries [36]. However, this substance represents a major problem for the environment because it is very toxic and difficult to degrade. Therefore, it is important to find an efficient and low-cost method to degrade it. Several methods of degradation are used today, including electrochemical degradation, biodegradation, and photochemical degradation [37]. However, these methods are either expensive

or slow. Recently, silver nanoparticles synthesized by green methods have been employed as an efficient alternative for degrading organic dyes [38–40]. Ashokkumar et al. degraded methylene blue with silver nanoparticles synthesized with a *Tribulus terrestris* leaf extract [40]. Thus, the present investigation carried out a synthesis of silver nanoparticles using an aqueous leaf extract of *A. triphylla*, and their catalytic activity against methylene blue was evaluated.

Materials and Methods

Materials and Plant Extract Preparation

Dried *A. triphylla* leaves collected from a local market in Morelia City, Méx., were used for the chemical reduction of AgNPs. Silver nitrate ($AgNO_3$) crystals, analytical grade, purchased from Meyer were used as the precursor salt in the biosynthesis. The precursor salt ($AgNO_3$) was used in an aqueous solution of 1, 3, and 5 mM concentrations. This aqueous solution was prepared using distilled water. The *A. triphylla* leaves were washed with distilled water to remove dust, and then they were milled in a ball mill SPEX 8000 M for 5 min. The aqueous extract was obtained by mixing 2 g of leaves with 100 ml of distilled water. The mix was heated at 80 °C for 30 min with magnetic stirring. The solution was filtered to separate the solid particles with Whatman filter paper # 41.

Synthesis of Silver Nanoparticles

The biosynthesis of AgNPs was performed by mixing 10 ml of the $AgNO_3$ solution with 10 ml of the *A. triphylla* leaves extract. The effect of the precursor salt concentration was evaluated by employing three levels (1, 3, and 5 mM). Another variable analyzed was the amount of the extract varying in 1, 2, 3, 4, and 5 ml. Consequently, the precursor salt/reducing agent relationship was changed. Moreover, the kinetics of the synthesis reaction was assessed at the reaction temperatures of 25, 50, 75, and 95 °C.

Characterization of Silver Nanoparticles and Catalytic Activity

Different structural characterization techniques were used to evaluate the synthesis of AgNPs. Uv–vis spectroscopy (Beckman DU-20 spectrophotometer) was accustomed to a rapid evaluation of the nanoparticles formation. Scanning electron microscopy (Jeol JSM 6700-F) and transmission electron microscopy (Phillips Tecnai F20 operating at a voltage of 200 keV) were employed to determine the size, morphology, and chemical composition of the samples containing AgNPs. X-ray diffraction analysis (Siemens D5000 diffractometer, CuKα radiation of 1.5406 Å) was carried out to determine the crystalline structure of dried samples. The study was conducted in an angular range of 20-80 °. FT-IR spectroscopy (Bruker Tensor 27 equipment with a resolution of 4 cm^{-1}) and Raman spectroscopy were performed to determine the kind of organic compounds involved in the reduction

and stabilization of the AgNPs. The catalytic activity of the AgNPs in the methylene blue degradation was evaluated. The analysis was carried out in 3.5 ml quartz cuvettes. One ml of 1×10^{-4} M methylene blue solution and 2 ml of the solution containing AgNPs were mixed in the cuvette. The catalytic activity of the nanoparticles was analyzed by Uv–vis, monitoring the changes in the absorbance band of methylene blue (645 nm).

Results and Discussion

Figure 1 shows the Uv–vis spectra of AgNPs synthesized at different concentrations of $AgNO_3$ with 5 ml of plant extract solution. The Uv–vis spectra showed an SPR absorption band located at 430 nm, suggesting the formation of AgNPs. It is observed that as the concentration of silver salt increases, the intensity of the absorption band decreases, indicating the lower density of the formed nanoparticles. The reduction in the intensity of the SPR band could be related to the increase in the particle size as a consequence of an increase in the bio-reduction rate when the precursor salt increased, needing more surfactant agents to impede the particle growth. In this way, *A. triphylla* leaf extract has the real capability of the Ag ions bioreduction, but it is limited to the AgNPs stabilization.

Figure 2a shows the SEM analysis of the AgNPs synthesized at different $AgNO_3$ concentrations. It found spherical nanoparticles at the concentration of 1 mM $AgNO_3$ (Fig. 2b). Moreover, at 3 mM $AgNO_3$, larger nanoparticles, some of them outside the nanometer range, were obtained. Finally, some agglomerates containing the AgNPs and residues of organic compounds at the concentration of 5 mM $AgNO_3$ were appreciated. Therefore, these results agree with the Uv–vis shown in Fig. 1.

The effect of the extract volume on the synthesis of AgNPs was also analyzed by varying in the range from 1 to 5 ml. All experiments were performed using a 3 mM $AgNO_3$ solution concentration. Figure 3 illustrates the Uv–vis results obtained for

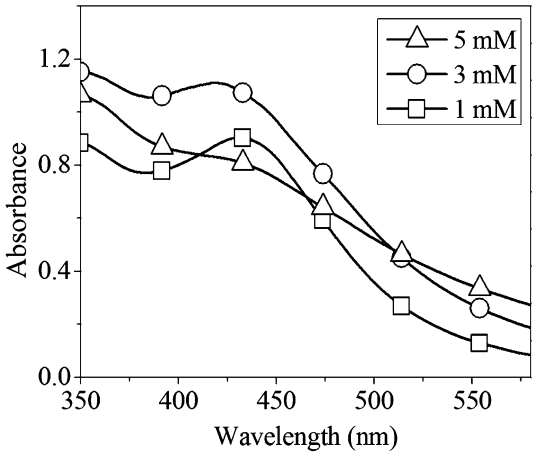

Fig. 1 UV–Vis spectra of the AgNPs synthesized with different $AgNO_3$ concentration solutions

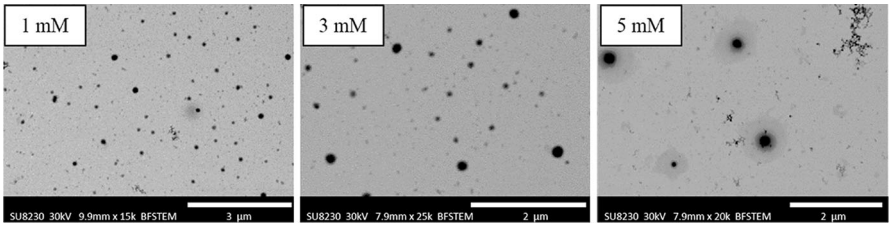

Fig. 2 SEM micrographs showing the size and morphology of the AgNPs varying the $AgNO_3$ concentration

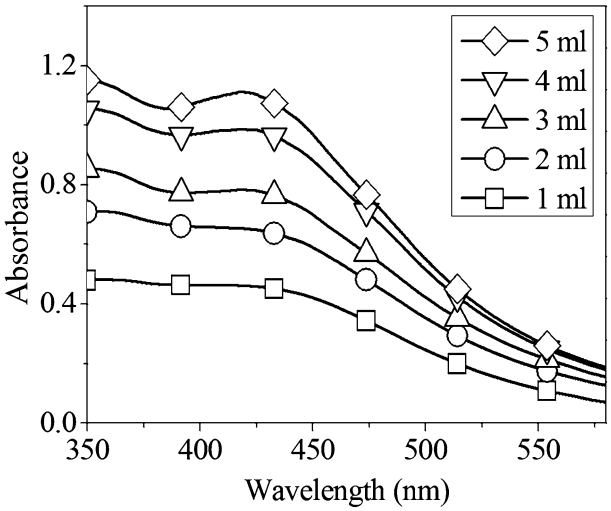

Fig. 3 UV–Vis spectra of the AgNPs synthesized with different extract volume

the different volumes of plant extract employed. A typical band of AgNPs, about 437 nm, was noted. As the plant extract concentration increased, the SPR band intensity was increased, indicating an increase in the density of silver nanoparticles formed. Moreover, the band shift toward shorter wavelengths showed a decrease of the formed AgNPs sizes. Thus, as the amount of *A. triphylla* extract increases, the concentration of the reducing agents and stabilizers becomes greater, leading to a further reduction and stabilization of the silver ions. Consequently, a higher concentration of AgNPs is formed. Similar results have been reported in several works [41–43].

Figure 4 shows Uv–vis results of the AgNPs synthesized at different temperatures. All spectra show an SPR absorption band of about 430 nm, which is typical of the AgNPs. Regardless of the temperature used, as the volume extract was increased, the SPR absorption band increased, indicating a greater concentration of nanoparticles. However, the band was broad in all spectra, suggesting a large size distribution. Therefore, the best results were observed when the reaction temperature was 95 °C, using 5 ml of *A. triphylla* extract. At this temperature, the

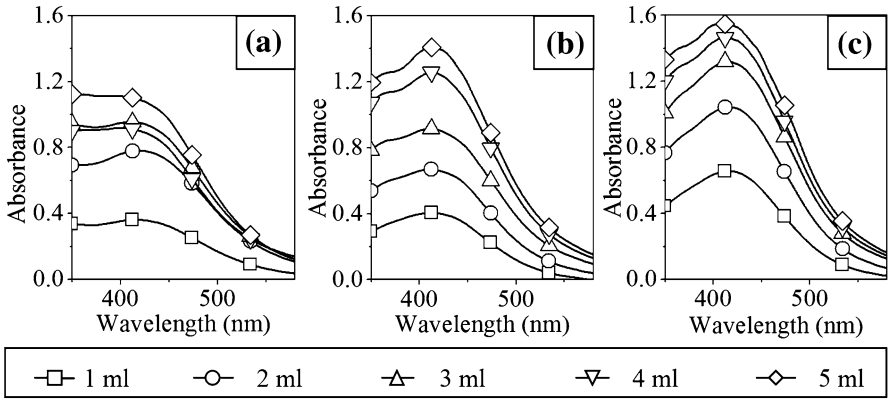

Fig. 4 UV-Vis spectra of the AgNPs synthesized at different reaction temperatures: **a** 50 °C, **b** 75 °C y **c** 95 °C

absorption band is greater and relatively narrower than the other samples, indicating nanoparticles with smaller ranges in size. However, in these spectra, a weak band centered at approximately 375 nm was observed, suggesting a bimodal size distribution. Ahluwalia et al. used five different temperatures, from 10 to 50 °C, and observed that absorbance increased as temperature increased [44]. This behavior occurs because as the reaction temperature increases, the bioreduction rate also increases. Therefore, a greater number of ions is consumed in the formation of nuclei, whereby a process of secondary reduction is avoided, resulting in the formation of smaller nanoparticles [45].

Studies by TEM were performed to corroborate the above results as shown in Fig. 5. The insets are the particle size distribution of AgNPs. Figure 5a shows a TEM micrograph that belongs to the sample performed at 50 °C. In this case, the morphology of AgNPs is nearly spherical with some irregular shapes. Moreover, a high-resolution transmission electron micrograph (Fig. 5b) shows the crystalline nature of the AgNPs. The measured distance of 0.23 nm corresponding to (111) planes of fcc-silver was observed. Figures 5b, c, illustrate AgNPs synthesized at 75 and 95 °C, showing an increase in nanoparticle sizes in comparison to the previous sample. It is clear that the morphology of the particles varied with the reaction temperature. In the last case, quasi-spherical, triangular and some irregularly shaped nanoparticles were observed. In addition, the nanoparticles size was greater than the other samples and had a clearly bimodal distribution. These experimental results are in agreement with those obtained by Uv–vis spectroscopy as shown in Fig. 4.

Figure 6 shows the X-ray diffraction patterns (XRD) of the nanoparticles prepared by biosynthesis. From the XRD pattern, the main diffraction peaks located at 37.96, 44.3, 64.5, and 77.44° correspond to the planes (111), (200), (220), and (311) of the Ag fcc structure. The silver XRD pattern was perfectly indexed with the 03-065-2871 card database number. Also, the peaks that are non-indexed are attributed to the organic compounds from the plant capping the silver nanoparticles. In several studies [46–48], the presence of organic compounds in the nanoparticles

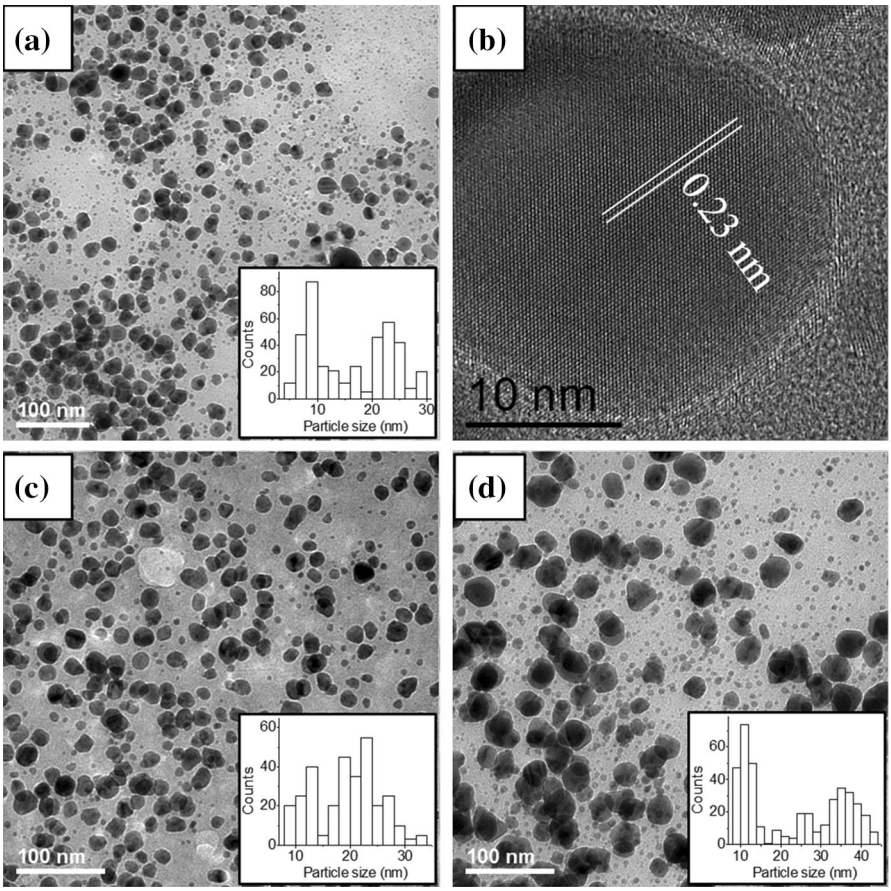

Fig. 5 TEM analysis of the AgNPs synthesized with *A. tripylla* extract at different temperatures: **a** 50 °C, **b** HRTEM micrograph showing the silver planes, **c** 75 °C, and **d** 95 °C (The *insets* show the particle size analysis)

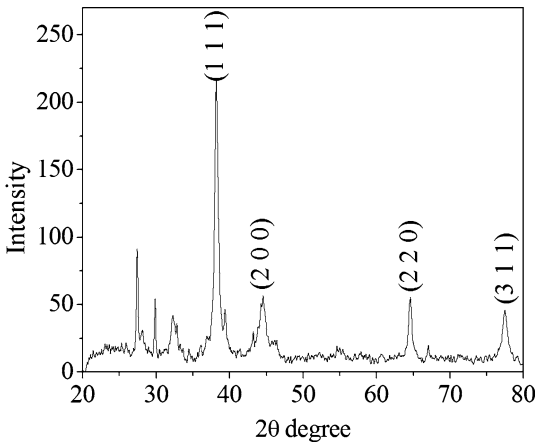

Fig. 6 X-Ray *diffractogram* of AgNPs synthesized with *A. triphylla* extract

synthesized has been reported. For example, Ulug et al. found some reflections between 20 and 30° belonging to organic compounds that encapsulated silver nanoparticles [46].

FT-IR analysis was performed to determine the chemical groups involved in the reduction and stabilization of the AgNPs. Figure 7a, b shows the FT-IR spectra of the *A. triphylla* leaves and the as-prepared AgNPs, respectively. In the *A. triphylla* leaves spectrum, seven bands appear; first, an O–H band at 3343 cm^{-1}, corresponding to phenolic groups from the extract, was observed. The band at 2924 cm^{-1} corresponds to C–H groups. According to Sre et al. the band centered at 1651 cm^{-1} is due to C=O bond of the amide compounds [49]. The C=C bond due to the aromatic compounds appears at 1410 cm^{-1}. The peak at 1255 cm^{-1} assigned to the N–H group from the amides and the band at 1073 cm^{-1} is attributed to the C–OH bond of the aromatic compounds. Finally, the band at 615 cm^{-1} can be assigned to the C–Cl bond as mentioned by Sadegui [50]. In the spectra corresponding to the sample after the synthesis of AgNPs, only some bands remain present: the bands corresponding to the phenolic compounds and amide groups. Thus, it can be suggested that these kinds of compounds involve the synthesis and capping of AgNPs. The reducing power of *A. triphylla* extract to synthesize AgNPs can be attributed to spathulenol, which is one of the mean substances in the leaves [34]. Spathulenol is a terpenoid compound with high reducing potential. Others compounds, reducer agents that can be associated with the synthesis of nanoparticles, are geranial and neral [34]. In all cases, these substances provide the electrons to reduce the Ag ion in Ag metal.

Figure 8 shows the Raman spectra of the AgNPs synthesized with 5 ml of *A. triphylla* extract. In the spectra is observed an intense band at 240 cm^{-1}. According to Mukherjee, this is attributed to Ag–N bonds [51]. Another band observed at 550 cm^{-1} corresponds to the C–Cl bond. The aromatic and amide bonds are centered at 1380 and 1610 cm^{-1}, respectively. These results confirm the involvement of amines and aromatic compounds in the capping process of the nanoparticles.

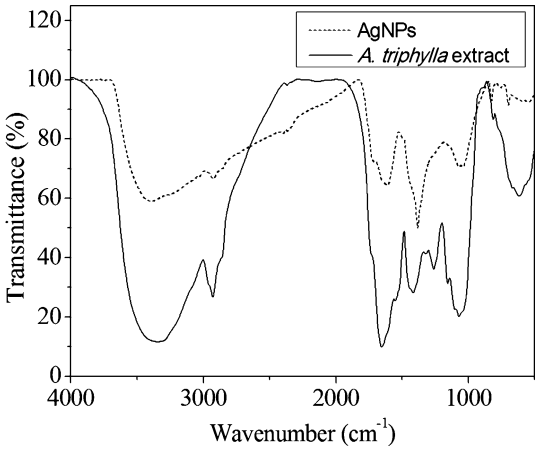

Fig. 7 FT-IR analysis of the *A. triphylla* extract and AgNPs

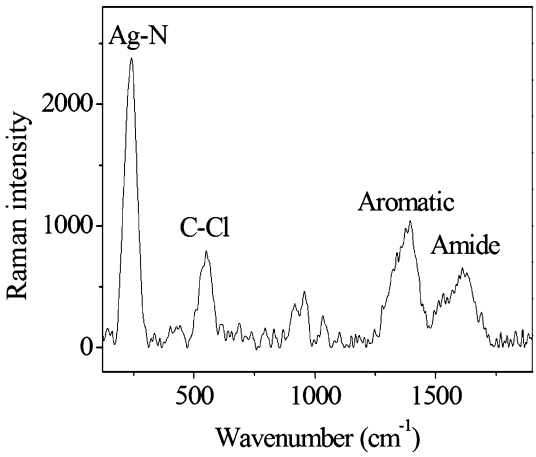

Fig. 8 Raman spectra of the AgNPs synthesized with *A. triphylla* extract

The degradation of methylene blue with the AgNPs synthesized with 5 ml of *A. triphylla* extract was observed in the Uv–vis spectra as shown in Fig. 9. As has been reported, the band corresponding to methylene blue appears at 664 nm [38–40]. For 30 min, the band intensity decreases, and this behavior is the same for 60 and 90 min. At the end of the reaction, the organic dye band showed a significant decrease in intensity, demonstrating the ability of AgNPs to degrade organic dyes. According to Tahir, the mechanism of the decomposition of methylene blue by silver nanoparticles is due to the radicals generated by electrons with high energy. This level of energy is obtained because the valence electrons of AgNPs are beaten by the light. After that, these electrons are emitted from the valence orbital of AgNPs, and then the reduction of methylene blue is carried out [39].

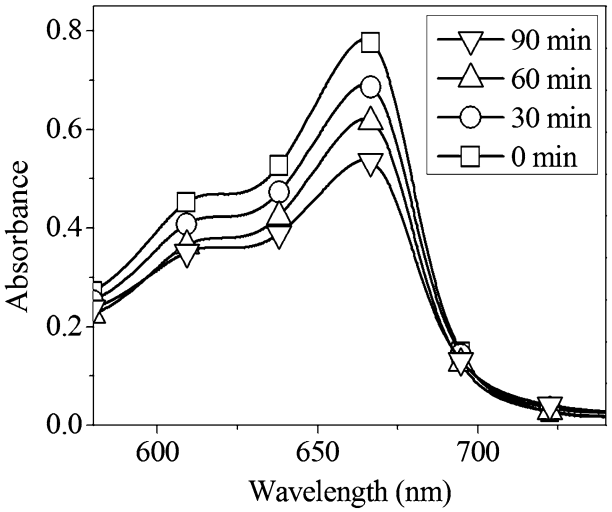

Fig. 9 UV–Vis spectra showing the methylene blue degradation in presence of AgNPs

Conclusions

AgNPs were obtained using *A. triphylla* leaf extract as a reducing agent and stabilizing agent at room temperature. The AgNPs were characterized by Uv–vis, XRD, SEM, FT-IR, RS, and TEM measurements. The Uv–vis analysis showed the surface plasmon resonance band around 430–445 nm, which is typical of the silver nanoparticles formation. The XRD technique confirms the presence of solids bio-reduced by the fcc structure of Ag. SEM and TEM observations showed spherical nanoparticles exhibiting size ranges of 5–40 nm. The FT-IR and Raman studies showed bands corresponding to phenolic compounds and the amide group involved in the synthesis and stabilization of AgNPs, respectively. The results also indicate that as the *A. triphylla* leaf extract/precursor salt ($AgNO_3$) ratio increases, the size of the nanoparticles decreases. Furthermore, as the reaction temperature increases, the reduction rate increases too, resulting in the formation of smaller nanoparticle size ranges. The Uv–vis results indicate that the AgNPs can reduce the methylene blue.

References

1. K. M. Kumara, M. Sinhaa, B. K. Mandala, A. R. Ghoshb, K. S. Kumarc, and P. S. Reddy (2012). *Spectrochim. Acta A* **91**, 228–233.
2. M. J. Ahmed, G. Murtaza, A. Mehmood, and T. M. Bhatti (2015). *Mater. Lett.* **153**, 10–13.
3. M. Ghaedi, M. Yousefinejad, M. Safarpoor, H. Z. Khafri, and M. K. Purkait (2015). *J. Ind. Eng. Chem.* **31**, 167–172.
4. V. Dehand, L. Soumya, S. Bharadwaj, S. Chakra, D. Bhatt, and B. Sreedhar (2016). *Mater. Sci. Eng. C* **58**, 36–43.
5. S. Pugazhendhi, P. Sathya, P. K. Palanisamy, and R. Gopalakrishnan (2016). *J. Photoch. Photobio. B* **159**, 155–160.
6. L. Wang, C. Liu, Y. Wang, H. Xu, H. Su, and X. Cheng (2016). *Curr. Appl. Phys.* **16**, 969–973.
7. P. R. R. Sre, M. Reka, R. Poovazhagi, M. Kumar, and K. Murugesan (2015). *Spectrochim. Acta A* **135**, 1137–1144.
8. K. Ramachandran, D. Kalpana, Y. Sathishkumar, Y. S. Lee, K. Ravichandran, and G. G. Kumar (2016). *J. Ind. Eng. Chem.* **35**, 29–35.
9. M. Nasrollahzadeh, S. M. Sajadi, F. Babaei, and M. Maham (2015). *J. Colloid Interf. Sci.* **450**, 374–380.
10. A. Rostami-Vartooni, M. Nasrollahzadeh, and M. Alizadeh (2016). *J. Alloy. Compd.* **680**, 309–314.
11. R. Mata, J. R. Nakkala, and S. R. Sadras (2015). *Mater. Sci. Eng. C* **51**, 216–225.
12. D. Dinesh, K. Murugan, P. Madhiyazhagan, C. Panneerselvam, P. M. Kumar, M. Nicoletti, W. Jiang, G. Benelli, B. Chandramohan, and U. Suresh (2015). *Parasitol. Res.* **114**, 1519–1529.
13. P. Madhiyazhagan, K. Murugan, A. N. Kumar, T. Nataraj, D. Dinesh, C. Panneerselvam, J. Subramaniam, P. M. Kumar, U. Suresh, M. Roni, M. Nicoletti, A. A. Alarfaj, A. Higuchi, M. A. Munusamy, and G. Benelli (2015). *Parasitol. Res.* **114**, 4305–4317.
14. J. Subramaniam, K. Murugan, C. Panneerselvam, K. Kovendan, P. Madhiyazhagan, P. M. Kumar, D. Dinesh, B. Chandramohan, U. Suresh, M. Nicoletti, A. Higuchi, J. S. Hwang, S. Kumar, A. A. Alarfaj, M. A. Munusamy, R. H. Messing, and G. Benelli (2015). *Environ. Sci. Pollut. Res.* **22**, 20067–20083.
15. A. Jaganathan, K. Murugan, C. Panneerselvam, P. Madhiyazhagan, D. Dinesh, C. Vadivalagan, A. T. Aziz, B. Chandramohan, U. Suresh, R. Rajaganesh, J. Subramaniam, M. Nicoletti, A. Higuchi, A. A. Alarfaj, M. A. Munusamy, S. Kumar, and G. Benelli (2016). *Parasitol. Int.* **65**, 276–284.
16. K. Rajarama, D. C. Aiswarya, and P. Sureshkumar (2015). *Mater. Lett.* **138**, 251–254.
17. Y. Mo, Y. Tang, S. Wang, J. Lin, H. Zhang, and D. Luo (2015). *Mater. Lett.* **144**, 165–167.

18. M. R. Bindhu and M. Umadevi (2015). *Spectrochim. Acta A* **135**, 373–378.
19. S. Ahmed, M. Ahmad, B. L. Swami, and S. Ikram (2016). *J. Adv. Res.* **7**, 17–28.
20. K. Vijayaraghavan and S. P. K. Nalini (2010). *J. Biotechnol.* **5**, 1098–1110.
21. K. N. Thakkar, S. S. Mhatre, and R. Y. Parikh (2010). *Nanomed. Nanotechnol. Biol. Med.* **6**, 257–262.
22. S. Patra, S. Mukherjee, A. K. Barui, A. Ganguly, B. Sreedhar, and C. R. Patra (2015). *Mater. Sci. Eng. C* **53**, 298–309.
23. V. Sujitha, K. Murugan, M. Paulpandi, C. Panneerselvam, U. Suresh, M. Roni, M. Nicoletti, A. Higuchi, P. Madhiyazhagan, J. Subramaniam, D. Dinesh, C. Vadivalagan, B. Chandramohan, A. A. Alarfaj, M. A. Munusamy, D. R. Barnard, and G. Benelli (2015). *Parasitol. Res.* **114**, 3315–3325.
24. S. Shivaji, S. Madhu, and S. Singh (2011). *Process Biochem.* **46**, 1800–1807.
25. A. Syed, S. Saraswati, G. C. Kundu, and A. Ahmad (2013). *Spectrochim. Acta A* **114**, 144–147.
26. K. Murugan, C. M. Samidoss, C. Panneerselvam, A. Higuchi, M. Roni, U. Suresh, B. Chandramohan, J. Subramaniam, P. Madhiyazhagan, D. Dinesh, R. Rajaganesh, A. A. Alarfaj, M. Nicoletti, S. Kumar, H. Wei, A. Canale, H. Mehlhorn, and G. Benelli (2015). *Parasitol. Res.* **114**, 4087–4097.
27. R. Rajan, K. Chandran, S. L. Harper, S. Yun, and P. T. Kalaichelvan (2015). *Ind. Crop. Prod.* **70**, 356–373.
28. G. Benelli (2016). *Parasitol. Res.* **115**, 23–34.
29. J. Song and B. Kim (2009). *Bioproc. Biosyst. Eng.* **32**, 79–84.
30. R. Amooaghaie, M. R. Saeri, and M. Azizi (2015). *Ecotox. Environ. Safe.* **120**, 400–408.
31. K. D. Arunachalam, S. K. Annamalai, and S. Hari (2013). *Int. J. Nanomed.* **8**, 1307–1315.
32. E. Zamorano-Ponce, C. Morales, D. Ramos, C. Sepulveda, S. Cares, P. Rivera, J. Fernandez, and M. A. Carballo (2006). *Mutat. Res.* **603**, 145–150.
33. A. Carnat, A. P. Carnat, D. Fraiss, and J. L. Lamaison (1999). *Fitoterapia* **70**, 44–49.
34. R. H. Olmedo, V. Nepote, and N. R. Grosso (2012). *J. Am. Oil Chem. Soc.* **89**, 2195–2205.
35. J. Grassmann (2005). *Vitam. Horm.* **72**, 505–535.
36. E. Rodríguez León, E. Larios Rodríguez, C. Rodríguez Beas, G. Plascencia-Villa, R.A. Iñiguez Palomares (2016) J. Nanomater. **2016** 10 pages.
37. T. Robinson, G. McMullan, R. Marchant, and P. Nigam (2001). *Bioresour. Technol.* **77**, 247–255.
38. S. Joseph and B. Mathew (2015). *J. Mol. Liq.* **204**, 184–191.
39. K. Tahir, S. Nazir, B. Li, A. U. Khan, Z. U. H. Khan, A. Ahmad, and F. U. Khan (2015). *Sep. Purif. Technol.* **150**, 316–324.
40. S. Ashokkumar, S. Ravi, V. Kathiravan, and S. Velmurugan (2014). *Spectrochim. Acta A* **121**, 88–93.
41. M. Ghaffari-Moghaddam and R. Hadi-Dabanlou (2014). *J. Ind. Eng. Chem.* **20**, 739–744.
42. S. P. Dubey, M. Lahtinen, and M. Sillanpää (2010). *Colloid Surf. A* **364**, 34–41.
43. S. M. Ghoreishi, M. Behpour, and M. Khayatkashani (2011). *Physica. E* **44**, 97–104.
44. V. Ahluwalia, J. Kumar, R. Sisodia, N. A. Shakil, and S. Walia (2014). *Ind. Crop. Prod.* **55**, 202–206.
45. N. Yang and W. H. Li (2013). *Ind. Crop. Prod.* **48**, 81–88.
46. B. Ulug, M. H. Turkdemir, A. Cicek, and A. Mete (2015). *Spectrochim. Acta A* **135**, 153–161.
47. G. Suresh, P. H. Gunasekar, D. Kokila, D. Prabhu, D. Dinesh, N. Ravichandran, B. Ramesh, A. Koodalingam, and G. V. Siva (2014). *Spectrochim. Acta A* **127**, 61–66.
48. M. Amin, F. Iram, M. S. Iqbal, M. Z. Saeed, M. Raza, and S. Alam (2013). *Carbohyd. Polym.* **92**, 1896–1900.
49. P. R. R. Sre, M. Reka, R. Poovazhagi, M. A. Kumar, and K. Murugesan (2015). *Spectrochim. Acta A* **135**, 1137–1144.
50. B. Sadeghi, A. Rostami, and S. S. Momeni (2015). *Spectrochim. Acta A* **134**, 326–332.
51. P. Mukherjee, M. Roy, B. P. Mandal, G. K. Dey, P. K. Mukherjee, J. Ghatak, A. K. Tyagiand, and S. P. Kale (2008). *Nanotechnology* **19**, 1–7.